Acta Crystallographica Section D
Biological Crystallography
ISSN 0907-4449

Four complete turns of a curved 3_{10}-helix at atomic resolution: the crystal structure of the peptaibol trichovirin I-4A in a polar environment suggests a transition to α-helix for membrane function

Renate Gessmann,[a] Danny Axford,[b] Robin L. Owen,[b] Hans Brückner[c,d] and Kyriacos Petratos[a]*

[a]IMBB–FORTH, N. Plastira 100, Heraklion, Crete 70 013, Greece, [b]Diamond Light Source Ltd, Harwell Science and Innovation Campus, Didcot OX11 0DE, England, [c]Research Center for BioSystems, Land Use and Nutrition (IFZ), Institute of Nutritional Science, Department of Food Science, University of Giessen, Heinrich-Buff-Ring 26-32, 65392 Giessen, Germany, and [d]Institute of Food Science and Nutrition, King Saud University, PO Box 2460, Riyadh 11450, Saudi Arabia

Correspondence e-mail: petratos@imbb.forth.gr

Received 27 July 2011
Accepted 29 November 2011

PDB Reference: trichovirin I-4A, 3sbn.

The first crystal structure of a member of peptaibol antibiotic subfamily 4, trichovirin I-4A (14 residues), has been determined by direct methods and refined at atomic resolution. The monoclinic unit cell has two molecules in the asymmetric unit. Both molecules assume a 3_{10} right-handed helical conformation and are significantly bent. The molecules pack loosely along the crystallographic twofold axis, forming two large tunnels between symmetry-related molecules in which no ordered solvent could be located. Carbonyl O atoms which are not involved in intramolecular hydrogen bonding participate in close van der Waals interactions with apolar groups. The necessary amphipathicity for biological activity of peptaibols is not realised in the crystal structure. Hence, a structural change of trichovirin to an α-helical conformation is proposed for membrane integration and efficient water/ion transportation across the lipid bilayer.

1. Introduction

Peptaibols are naturally occurring microheterogen peptides of fungal origin consisting of up to 20 residues. They are acetylated at the N-terminus and possess a C-terminal 2-amino alcohol. The nonstandard helix-promoting α-aminoisobutyric acid (Aib) is frequently present in the sequence. Peptaibols have been assigned certain types of bioactivity and membrane-modifying properties. These include bactericidal effects against *Staphylococcus aureus* and *Escherichia coli*, fungicidal activity against *Sclerotium cepivorum* and membrane-modifying properties such as the permeabilization of liposomes prepared from phosphatidylcholine and cholesterol, as well as concentration-dependent and voltage-dependent ion conductance in lipid membranes (Rebuffat *et al.*, 1995). The 14-mer to 20-mer peptaibols are synthesized by large multi-subunit nonribosomal peptide synthetases, which represent the largest enzymes known to date (Mukherjee *et al.*, 2011; Wiest *et al.*, 2002). Peptaibols form multimeric transmembrane channels through self-association. These channels are able to conduct ionic species, leading to loss of osmotic balance, lysis and thus cell death of the host. Trichovirin I-4A is a 14-residue peptaibol antibiotic from *Trichoderma viride* strain NRRL 5243 (Kiess & Brückner, 1990). The sequence of trichovirin I-4A (acetyl-Aib-Asn-Leu-Aib-Pro-Ala-Val-Aib-Pro-Aib-Leu-Aib-Pro-Lol; symbols for nonstandard residues are given in the legend to Fig. 5) is identical to that of harzianin HC-VI from *T. harzianum* M-903603 (Lucaciu *et al.*, 1997; Rebuffat *et al.*, 1995). *Trichoderma* strains are known to induce plant defence and are used as biocontrol agents (Viterbo *et al.*, 2007).

Peptaibols have been divided into subfamilies (SFs) on the basis of their length, sequence and functional properties

© 2012 International Union of Crystallography
Printed in Singapore – all rights reserved

(Chugh & Wallace, 2001). Crystal or solution NMR structures of members of some subfamilies have been determined (Balashova *et al.*, 2000; Chugh *et al.*, 2002; Fox & Richards, 1982; Karle *et al.*, 1998; Snook *et al.*, 1998), but no crystal structure of a member of SF4 is known to date. Here, we report the first structure of a peptaibol that belongs to SF4. This subfamily consists of peptaibols with either 11 or 14 residues. In position 2 there is a conserved Asn or Gln residue and the members with 14 residues possess Pro at positions 5, 9 and 13. Neither aromatic nor charged residues are present. These peptaibols form channels despite their limited number of residues, which thus results in short helices. The hydrocarbon region of the bilayer membrane spans approximately 30 Å. However, in agreement with the mattress model of lipid–peptide interaction (Mouritsen & Bloom, 1984), a degree of length mismatch is tolerated, implying local distortion of the bilayer. The two molecules in the asymmetric unit described here form curved helices which assume a 3_{10}-helical conformation and measure 25.8 and 24.0 Å in length. A peptide adopting a 3_{10}-helical conformation is longer than in the respective α-helical conformation. Nevertheless, in the reported structures the helical bend is more than 60° and shortens the length of these 3_{10}-helices.

2. Materials and methods

2.1. Synthesis

Trichovirin I-4A was chemically synthesized by conventional stepwise segment condensation of protected peptides using benzyloxycarbonyl (Z) as an N-terminal protecting group, *tert*-butyl ester (O*t*Bu) or methyl ester (OMe) for C-terminal protection and 1-hydroxybenzotriazole (HOBt) and water-soluble carbodiimide (EDC.HCl) as coupling reagents. The purity of the final product and its stereochemical identity with the natural trichovirin I component 4A was proven by thorough analytical characterization using high-performance liquid chromatography, electrospray ionization mass spectrometry, chiral gas chromatography–mass spectrometry, optical rotation and elemental analysis (Brückner & Koza, 2003).

2.2. Crystallization and data collection

Trichovirin crystals were produced from a methanol–acetonitrile–water mixture and are colourless hair-like objects with a smallest dimension of about 30 µm (Supplementary Fig. S1[1]). Crystals were mounted by hand onto Micromesh (MiTeGen) sample supports. Diffraction data were collected at 100 K at the Diamond Light Source in Didcot, England on the microfocus beamline I24 (Evans *et al.*, 2011) using a Pilatus 6M detector (Dectris Ltd, Baden, Switzerland; Kraft *et al.*, 2009). The X-ray beam was focused to a size of 10 µm full-width half-maximum using two pairs of Kirkpatrick–Baez mirrors. The morphology of the crystals allowed data to be collected at a number of positions along their length, which enabled the best diffracting regions to be identified. A data set of 1500 images covering a 375° rotation was collected from a single trichovirin crystal. Data were integrated using the software package *XDS* (Kabsch, 2010) and scaled using *SCALA* (Evans, 2006), which is incorporated in the *CCP*4 program suite (Winn *et al.*, 2011). The data-set statistics are summarized in Table 1.

Table 1
Data-collection, processing and refinement statistics.

Values in parentheses are for the outermost resolution shell.

Space group	$P2_1$
Unit-cell parameters (Å, °)	a = 24.28, b = 9.90, c = 37.57, β = 97.15
Wavelength (Å)	0.7469
Resolution range (Å)	37.3–0.9 (0.95–0.90)
No. of measured reflections	86686 (11008)
No. of unique reflections	13524 (1868)
$\langle I/\sigma(I)\rangle$	13.2 (3.1)
Average multiplicity	6.4 (6.2)
Completeness (%)	98.4 (91.6)
$R_{\rm p.i.m.}$†	0.028 (0.257)
$R_{\rm meas}$‡	0.072 (0.654)
R factor (%)	
Without σ cutoff	10.2 (21.9)
For reflections with $F_{\rm o} > 4\sigma$	9.6 (16.4)
$R_{\rm free}$§ (%)	
Without σ cutoff	12.8
For reflections with $F_{\rm o} > 4\sigma$	12.2
No. of non-H atoms in a.u.¶	196
No. of solvent molecules in a.u.¶	14.5
R.m.s. deviations from ideal values	
Bond lengths (1,2 distances, 31 restraints) (Å)	0.045
All bond lengths, restrained and unrestrained (Å)	0.036
Bond angles (1,3 distances, 12 restraints) (Å)	0.076
All bond angles, restrained and unrestrained (°)	3.6
Average B factor (Å^2)	
Mol-*A*, main/side chain	8.7/11.6
Mol-*B*, main/side chain	9.2/12.2
Solvent atoms	20.9
Ramachandran plot	
Residues in the most favoured region (%)	100

† $R_{\rm p.i.m.}$ is the multiplicity-weighted precision-indicating merging R factor for comparing symmetry-related reflections (Weiss & Hilgenfeld, 1997). ‡ $R_{\rm meas}$ is the redundancy-independent multiplicity-weighted R factor for comparing symmetry-related reflections (Diederichs & Karplus, 1997). § $R_{\rm free}$ is calculated for a test set consisting of a random 5% of the diffraction data. ¶ a.u., asymmetric unit.

2.3. Structure determination and refinement

The structure was solved by direct methods by means of the program *ACORN* (Jia-xing *et al.*, 2005) using all reflections, starting from random phases and searching for 180 peaks with density above 4 r.m.s. deviations. A β-turn fragment comprising 18 atoms was located, in which one Aib C^{α} atom was identified by the four non-H atoms bonded to it. The structure was further defined by trying several input choices with the program *ARP*/*wARP* (Perrakis *et al.*, 1997), which resulted in the location of 164 atoms of 26 residues in both molecules [termed molecule *A* (mol-*A*) and molecule *B* (mol-*B*)] of the asymmetric unit. The model was completed manually to include all 196 non-H atoms by inspection of $2F_{\rm o} - F_{\rm c}$ and difference Fourier maps using *XtalView* (McRee, 1999). The structure was refined using the program *SHELXL* (Sheldrick, 2008). Rigid-body refinement using both mole-

[1] Supplementary material has been deposited in the IUCr electronic archive (Reference: KW5037). Services for accessing this material are described at the back of the journal.

cules as rigid bodies with data between 10 and 2 Å resolution produced an R factor of 25.3% and an R_{free} of 28.3%. Unrestrained refinement with antibumping restraints led to an R factor and R_{free} of 21.1% and 22.4%, respectively. Introduction of solvent molecules (ten fully occupied and six half-occupied water molecules, two methanol molecules and two acetonitrile molecules, with the latter four molecules having limited occupancies), anisotropic temperature-factor refinement and modelling of four disordered side chains [Val7 in both molecules, Leu11 (mol-*B*) and Lol14 (mol-*A*)] and the introduction of riding H atoms produced an R factor of 10.7% and an R_{free} of 13.5%. In the last 20 cycles of refinement the 25 most disagreeable reflections were omitted, which led to a final R factor of 9.6% and an R_{free} of 12.2% for reflections with $F_o > 4\sigma$. Most of the omitted reflections belong to the ($h0l$) plane. The structure exhibits relatively high values of anisotropic displacement parameters in the *ac* plane. Therefore, a small fraction of the respective calculated centric structure factors deviate significantly ($>5\sigma$) from the observed values. In total, 2134 parameters were refined against 13 524 reflections. The following restraints were used: distance and angle restraints for three of the four disordered side chains and Lol14 (mol-*B*), as well as for the methanol and acetonitrile molecules. 31 restraints for bonds (1,2) and 12 restraints for angles (1,3) were used (a further 474 possible distance restraints were not applied), together with DELU and SIMU restraints on thermal displacement parameters of bonded atoms for all non-H atoms and ISOR 'approximately isotropic' restraints for the solvent molecules, giving a total of 2263 restraints. R.m.s. deviations from ideality (Engh & Huber, 2006) for the restrained and for all bonds and angles are given in Table 1.

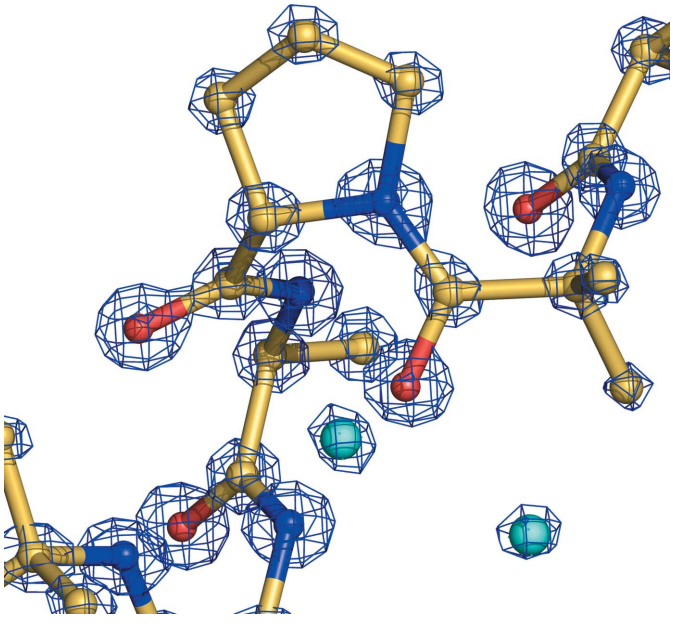

Figure 1
Electron density of the $2F_o - F_c$ map contoured at 4σ (blue) around Pro5 in mol-*A*. Two water molecules are shown in cyan.

The validation server of the Protein Data Bank (Berman *et al.*, 2006; Laskowski *et al.*, 1993) as well as *Mogul* from the Cambridge Crystallographic Data Centre (Taylor, 2002; Bruno *et al.*, 2004) were used to examine the quality of the structure. *MolProbity* (Chen *et al.*, 2010) was used for rotamer and clashscore calculations. *SwissPDBViewer* (Guex & Peitsch, 1997; http://spdbv.vital-it.ch/), *POV-Ray* (Persistence of Vision Pty Ltd, 2004), *PyMOL* (DeLano, 2002) and *VMD* (Humphrey *et al.*, 1996) were used for geometric analysis, visualization and for the production of figures and movies.

3. Results

3.1. Molecular structure

The quality of the refined structure at the atomic level is reflected in the electron-density map shown in Fig. 1. Two independent molecules (*A* and *B*) were located in the asymmetric unit of the crystal. In Fig. 2 and Supplementary Movie 1, a superposition of the two independent molecules is shown. Both chains adopt a curved 3_{10}-helical conformation stabilized by intramolecular hydrogen bonds. Both 3_{10}-helices have four complete turns. The imino groups of the three proline residues per molecule cannot participate in hydrogen bonding. Therefore, the number of possible intramolecular 4→1 hydrogen bonds in peptides of equal length that consist exclusively of nonproline residues is reduced from 12 to nine. Nine hydrogen bonds are indeed formed in both molecules (Fig. 2). The hydrogen bond between the C═O group of Aib1 (mol-*B*) and the NH group of Aib4 (mol-*B*) is remarkably weak and is less linear than all other intramolecular hydrogen bonds in both molecules. There is another hydrogen bond (5→1 type) formed at the N-terminus of mol-*B*. This 5→1 hydrogen bond involves the acetyl group and Aib4 (mol-*B*) and is longer than the 4→1 hydrogen bond between the acetyl group and Leu3 (mol-*B*). Fig. 3 shows the backbone confor-

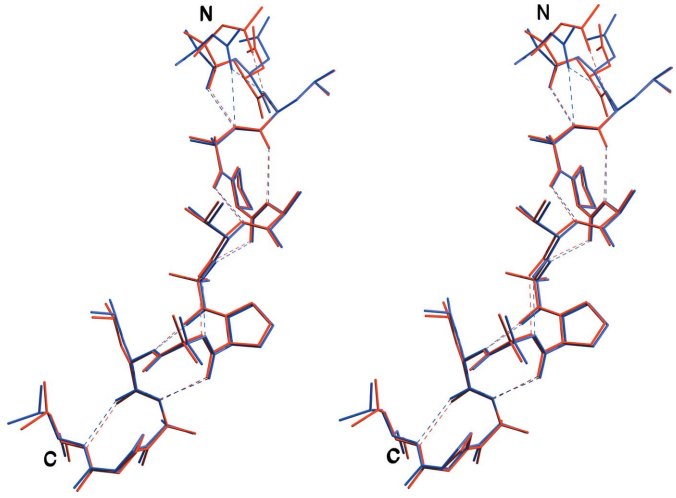

Figure 2
Wall-eyed stereoview of the superposition of mol-*B* (blue) on mol-*A* (red). Hydrogen bonds are shown in orange for mol-*A* and light blue for mol-*B*. N and C denote the amino-termini and reduced carboxy-termini of the molecules, respectively.

mation and the hydrogen-bonding pattern for mol-*A* (red) and mol-*B* (blue). Among other things, the interruption in the hydrogen-bonding pattern resulting from the presence of prolines is apparent. Other clearly visible features are variations in the conformation angles, hydrogen-bond type and distance. In particular, the existence of a bifurcated hydrogen bond is denoted as two symbols on the same residue (residue *i* as described in the figure legend) in the same colour below the 3.5 Å line (the chosen distance limit for hydrogen bonding), as seen for the N-terminal of mol-*B*.

Apart from the variation at their N-termini, molecules *A* and *B* are very similar (Figs. 2 and 3). The r.m.s. displacement between all non-H atoms is 0.53 Å (maximum of 2.7 Å). This value is reduced to 0.19 Å (maximum of 0.7 Å) on starting the comparison at Leu3 and decreases to 0.12 Å (maximum of 0.3 Å) when the main-chain atoms of residues 3–14 are selected.

A simple observation in the graphics shows that a small change of 11° in the φ conformation angle of Asn2 (mol-*B*) elongates the 5→1 hydrogen bond between the acetyl group (mol-*B*) and Aib4 (mol-*B*) to more than 3.5 Å, the limit for hydrogen bonding. If this change is applied to mol-*B* the mixed helix becomes a pure 3_{10}-helix.

The peptide consists of Xaa-Yaa-Aib-Pro tetrapeptide units, which are repeated three times. One such tetrapeptide unit forms a ribbon of overlapping β-turns twisted into a spiral. The helices of both molecules are not regular, but vary in both φ and ψ values from residue to residue at the same position inside the tetrapeptide unit (Fig. 3). Owing to the stereochemical restriction of Aib to the helical region, the usual residues adopt conformation angles close to the limit of the allowed helical region. The extreme values are found in the branched side-chain residues (Leu3, Val7, Leu11 and Lol14).

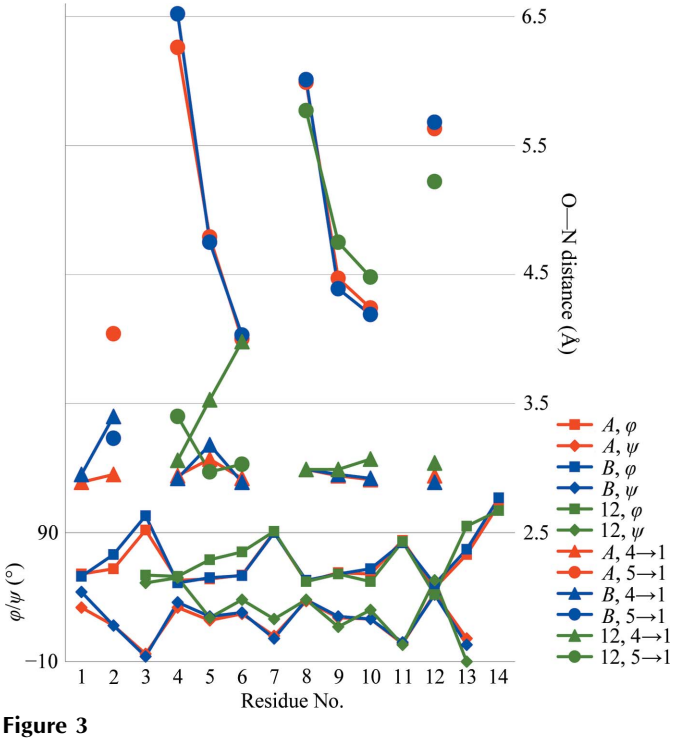

Figure 3
Structural parameters for trichovirin mol-*A* and mol-*B* and for the C-terminal dodecapeptide of trichovirin (Gessmann *et al.*, 1999), plotted in red, blue and green, respectively. The left-hand *y* axis shows the opposite signed dihedral angles at residue *i* associated with the squares (φ) and diamonds (ψ). The right-hand *y* axis shows the distance at residue *i* between the carbonyl of $i-1$ and the NH of $i+2$ (4→1; triangles) and the distance at residue *i* between the carbonyl of $i-2$ and the NH of $i+2$ (5→1; circles). Detailed values are given in Supplementary Tables S1 and S2.

Table 2
Matthews coefficients (V_M; Matthews, 1968) and solvent contents of peptaibol structures solved by X-ray crystallography.

Peptaibol	Reference	PDB code	Matthews ratio (Å^3 Da^{-1})	Solvent content [%(*v*/*v*)]
Trichovirin I-4A	Present work	3sbn	1.61	23.8
Alamethicin F-30	Fox & Richards (1982)	1amt	1.55	21.0
Trichotoxin A50E	Chugh *et al.* (2002)	1m24	1.44	14.5
Antiamoebin I	Snook *et al.* (1998)	1joh	1.41	12.8

3.2. Crystal packing

The located waters in the crystal structure (ten fully occupied, six half occupied) form three clusters (I, II and III) comprising seven, seven and two molecules, respectively.

Molecules *A* are hydrogen bonded head-to-tail, directly and *via* one water molecule of the first cluster (I). Members of the same cluster connect to molecules *A* shifted along the *b* axis. Layers are thus formed parallel to the *ab* plane. In Fig. 4(*b*) the lower right orange–red–orange coloured molecules (*A*) are members of such a layer.

The head-to-tail hydrogen bonding in molecules *B* is mediated by a water molecule from the second water cluster (II). This forms a bifurcated bond to the C-terminal O atoms. Similar to the head-to-tail hydrogen bonding of molecules *A*, a second water-mediated hydrogen bond connects to a *B* molecule translated along the *b* axis. The layers of molecules *B* stack parallel to the layers of molecules *A*, while the direction of the curved helical axis in one layer adopts a near-right angle with respect to the other layer.

One mol-*A* is hydrogen bonded to one mol-*B* at the N-terminal region. There is one direct hydrogen bond between the two Asn2 side chains and three 'Asn2 side chain to backbone' hydrogen bonds mediated by water molecules. This leads to a pairwise arrangement of the head-to-tail hydrogen-bonded layers of one layer *A* and one layer *B* in the *z* direction (Supplementary Fig. S2 and Supplementary Movie 2).

The two space-group symmetry (screw-axis) related layers of molecules *A*, like the corresponding layers of molecules *B*, form the closest van der Waals contacts (3.2 Å) with the convex middle part of the molecules. Among the groups which are involved in these close contacts are the carbonyl groups Ala6 and Aib10, which do not participate in any hydrogen bonding.

Further details concerning hydrogen bonding (Table S2) and crystal-packing visualization are provided in the Supplementary Material.

3.3. Solvent content

An interesting feature is the calculated high solvent content in the crystal of trichovirin in comparison with other peptaibols (Table 2). Assuming a van der Waals volume of 20.58 Å^3 (Li & Nussinov, 1998) for a water molecule, there is space available for ∼50 water molecules in the asymmetric unit. The ordered solvent found in electron-density maps is less than a third of that expected. Looking along the *b* axis in the crystal, there appears to be two empty channels (highlighted ellipses in Fig. 4*b*) with diameters of about 8.2 and 11.5 Å, each formed by every four symmetry-related *A* and *B* molecules. The poor electron density inside these channels was interpreted as two half-occupied methanol molecules which are hydrogen bonded and as two isolated acetonitrile molecules with low occupancy. Along the other two crystal axes the molecules are much more compactly packed (Figs. 4*a* and 4*c*).

3.4. Comparison to the C-terminal fragments of trichovirin I-4A

The structures of the benzyloxycarbonyl (Z) protected C-terminal tetrapeptide with two molecules in the asymmetric unit and the C-terminal octapeptide and dodecapeptide have been determined (Gessmann *et al.*, 1994, 1999). A significant difference between these peptides and trichovirin I-4A is their propensity to form crystals. Only the complete peptaibol was difficult to crystallize as regards time and resulting crystal size.

Moreover, the tetrapeptides and the octapeptide form 3_{10}-helices, while the dodecapeptide folds with five 4→1 3_{10}-helical and three 5→1 α-helical hydrogen bonds, thus forming a mixed helix (green symbols in Fig. 3).

The r.m.s. displacements between the main-chain atoms of the dodecapeptide and the corresponding atoms in molecules *A* and *B* are 1.25 and 1.23 Å, respectively. The greatest differences (of up to 4 Å) lie where the three 5→1-type hydrogen bonds are formed in the dodecapeptide.

The bend angle (see Table 3 for definition) of the dodecapeptide is 57.4° and is thus 6° and 7° lower than those of the complete peptaibol peptides. This fact, together with the observed different hydrogen-bonding pattern, is probably the reason that a model based on the dodecapeptide structure was unsuitable for the determination of the structure of full-length trichovirin by molecular replacement.

4. Discussion

The backbone conformation angles φ/ψ of trichovirin I-4A differ from those of a regular 3_{10}-helix with torsion angles of −57/−30° (Toniolo & Benedetti, 1991) and the torsion angles φ/ψ of the β-bend ribbon spiral (BBRS), which is an approximate 3_{10}-helix with a hydrogen-bond donor every two

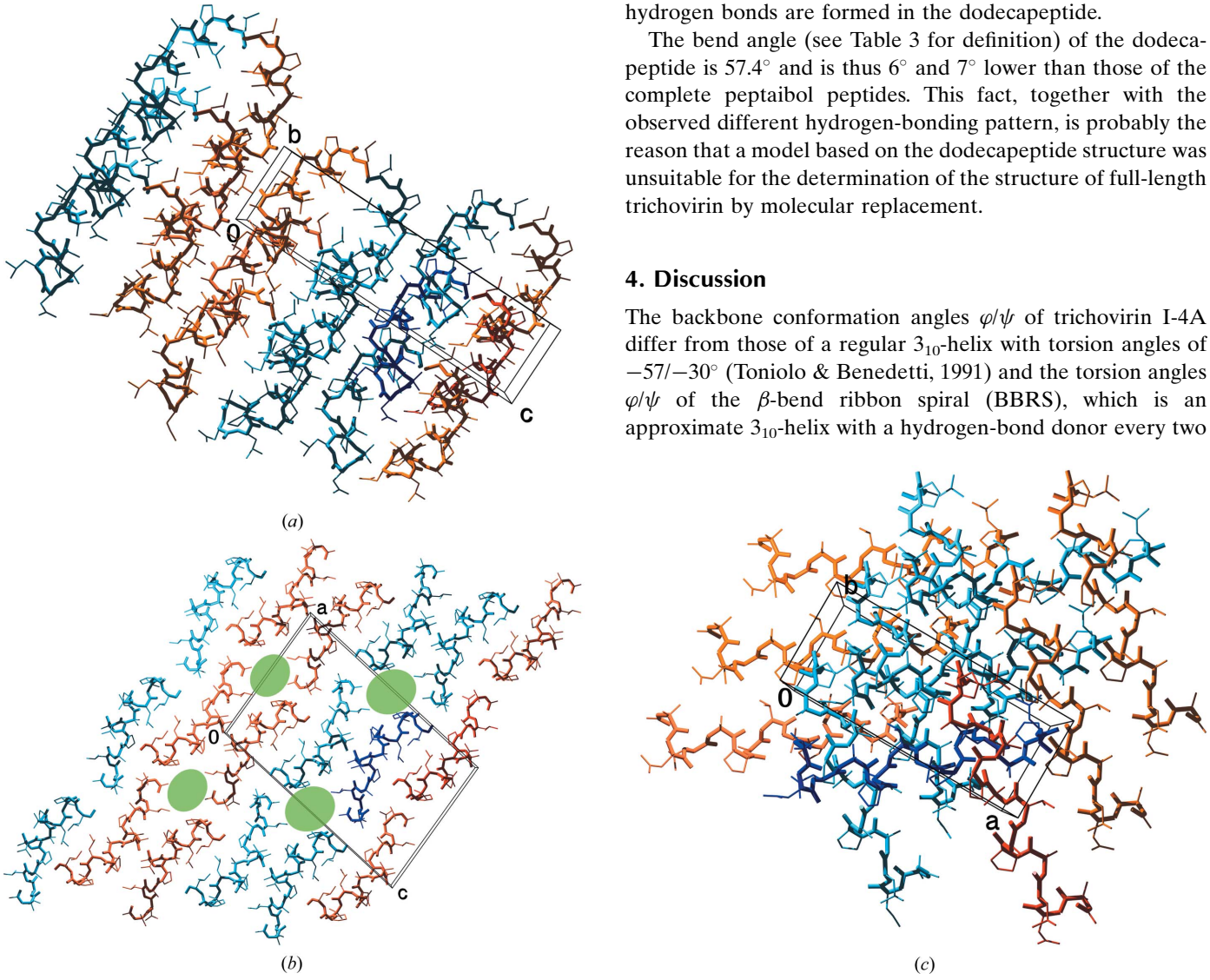

Figure 4
Arrangement of the molecules in the crystal: mol-*A* in red and mol-*B* in blue. The asymmetric unit is shown in darker colours. Side chains are denoted by thin lines; solvent atoms are omitted for clarity. (*a*) View along the *a* axis; one molecule layer is shown in the *bc* plane. (*b*) View along the *b* axis; one molecule layer is shown in the *ac* plane and empty bulk-solvent channels are shown as green ellipses. (*c*) View along the *c* axis; one molecule layer is shown in the *ab* plane.

Table 3
Geometric parameters of peptaibol structures solved by X-ray crystallography and NMR.

Peptaibol/family	No. of residues	Length† (Å)	Bend angle‡ (°)	*n*§	*h*§ (Å)	Pitch§ (Å)	Dipole moment¶ (D)
Trichovirin/SF4	14						
Mol-*A*		25.8	63.5	3.22	1.95	6.28	25.8
Mol-*B*		24.0	64.2	3.28	1.91	6.26	26.0
Zervamicin (Balashova *et al.*, 2000)/SF3 (13)††	16	25.9	47.0	3.57	1.56	5.57	31.8
Antiamoebin (Snook *et al.*, 1998)/SF2	16						
Mol-*A*		28.3	56.0	3.55	1.65	5.86	29.1
Mol-*B*		28.6	48.5	3.51	1.67	5.86	28.7
Second crystal structure (Karle *et al.*, 1998)		28.1	53.4	3.54	1.73	6.12	32.5
Trichotoxin (Chugh *et al.*, 2002)/SF1	18						
Mol-*A*		30.4	12.1	3.55	1.64	5.82	35.4
Mol-*B*		27.8	13.4	3.58	1.60	5.73	33.1
Alamethicin (Fox & Richards, 1982)/SF1	20						
Mol-*A*		33.7	33.3	3.62	1.63	5.90	51.8
Mol-*B*		31.6	29.6	3.60	1.61	5.80	50.2
Mol-*C*		32.0	21.5	3.56	1.61	5.73	50.0
α-Helix				3.60	1.50	5.40	
3_{10}-Helix (Toniolo & Benedetti, 1991)				3.24	1.94	6.29	
BBRS (Di Blasio *et al.*, 1992)				3.43	2.06	7.07	
Xaa-Yaa-Aib-Pro (Ségalas *et al.*, 1999)			38.6	3.56	1.72	6.12	

† Distance from the more distant atom (CH_3 or O) of the acetyl protection group to the O of the C-terminal amino alcohol. ‡ Angle between the planes on either side of the 'central Pro/Hyp' residue *n* (Fig. 5) formed by N atoms of residues $n-2, n-4, n-6$ (plane 1) and residues $n+1, n+3, n+5$ (plane 2), as proposed by Snook *et al.* (1998). § *n*, average number of residues per turn; *h*, average unit height in the helix; pitch, $n \times h$; calculated with *HELANAL* (Bansal *et al.*, 2000) after substituting all unusual residues with conventional residues. ¶ Calculated using the *Protein Dipole Moments Server* (http://bioinfo.weizmann.ac.il/dipol/) after substituting all unusual residues with conventional residues; units are Debyes (1 D = 0.20819 e Å). †† Most representative model of the NMR structure ensemble 1dlz chosen by the *OLDERADO* tool of the Protein Data Bank at EBI (Kelley *et al.*, 1997).

Trichovirin I-4A Ac-U-N-L-U-P-A-V-U-P-U-L-U-P-Lol
Zervamicin IIB[1] Ac-W-I-Q-J-I-T-U-L-U-Q-Q-U-O-U-P-Fol
Antiamoebin[2,3] Ac-F-U-U-U-J-G-L-U-U-Q-Q-J-O-U-P-Fol
Trichotoxin A40_1[4] Ac-U-G-U-L-U-Q-U-U-U-A-A-U-P-L-U-U-Q-Vol
Alamethicin[5] Ac-U-P-U-A-U-A-Q-U-V-U-G-L-U-P-V-U-U-E-Q-Fol

Figure 5
Sequences of peptaibols for which structures have been solved by X-ray crystallography or NMR. 1, Balashova *et al.* (2000); 2, Snook *et al.* (1998); 3, Karle *et al.* (1998); 4, Chugh *et al.* (2002); 5, Fox & Richards (1982). U, Aib (α-aminoisobutyric acid); O, Hyp (4-hydroxyproline); J, Iva (isovaline); Lol, leucinol; Fol, phenylalaninol; Vol, valinol). The 'central' Pro/Hyp is underlined.

residues, *e.g.* $(\text{Aib-Pro})_n$ dipeptide repeats, for which φ/ψ angles of $-54/-40^\circ$ (Aib) and $-78/-10^\circ$ (Pro) have been reported (Di Blasio *et al.*, 1992). For harzianin HC IX, which differs from the trichovirin sequence at two residues, a new spiral type, the (Xaa-Yaa-Aib-Pro)-β-bend ribbon spiral, has been proposed (Ségalas *et al.*, 1999) based on 60 modelled structures generated from NOE-derived interproton distance constraints (in methanol solution), with four calculated φ/ψ conformation angles. These conformation angles also differ substantially from the average conformation angles of molecules *A* and *B*.

Therefore, it is obvious that the conformational angles φ/ψ are not sufficient to classify the exact type of helical secondary-structure element.

We calculated geometric parameters uniformly for the crystal structures and one solution NMR structure of selected published peptaibols (Fig. 5 and Table 3). Based on these, it is clear that the two trichovirin peptides are the shortest in the sample, while their bend angles are the largest determined to date. As regards the helical geometry parameters, it is also clear that both molecules *A* and *B* of trichovirin should be classified as 3_{10}-helical. Hence, trichovirin I-4A is to our knowledge the longest peptide right-handed 3_{10}-helix for which a crystal structure has been determined. Trichovirin also possesses the lowest dipole moment of these peptaibols, which is a consequence not only of the shorter length but also of the high bend angle, which results in misalignment of the single dipole moment vectors.

A theoretical model of a peptide derived from the conformation angles given for the closely related harzianin HC IX in methanol (Ségalas *et al.*, 1999) results in a structure with a bend angle of only 38.6° and 3.56 residues per turn, a height per residue of 1.72 Å and a helical pitch of 6.12 Å. These values do not agree with the those determined experimentally here.

The structures of some long 3_{10}-helical peptides have been determined. Aib homopeptides, the longest described to date (Gessmann *et al.*, 2003), form 3_{10}-helices. The incorporation of one medial Gly residue in a Phe-Aib_{16} peptide only perturbs the regularity of the left-handed 3_{10}-helix in its vicinity (Solà *et al.*, 2011).

Trichovirin has 5/14 Aib residues, or about 36% Aib content. In the past, a peptaibol with this Aib content (<50%) and of more than eight residues in length would be expected to form an α-helix (Toniolo & Benedetti, 1991). The observed 3_{10}-helical structure enables the spanning of a distorted membrane better than an α-helical structure, as 3_{10}-helices are thinner and longer than α-helices. Nevertheless, the 60° bend shortens the length considerably.

5. Implications

Conclusions about the possible multimeric arrangement of the peptides in the bilayer membrane can be drawn by investigating the distribution of the polar groups which do not participate in intramolecular hydrogen bonding and the relative position of the apolar groups (Sansom, 1991; Chen *et al.*, 2005). The apolar groups are usually thought to contact the hydrophobic membrane, while the free carbonyl groups (those not involved in intramolecular hydrogen bonding) of the peptide point inside the hydrophilic ion channel. The intermolecular arrangement of peptaibols is usually attributed to the N- and C-terminal polar groups. The intermolecular crystal packing described here with channels along the *b* axis is unlikely to reflect the situation in the membrane, as the free carbonyl groups contact apolar groups and the channels

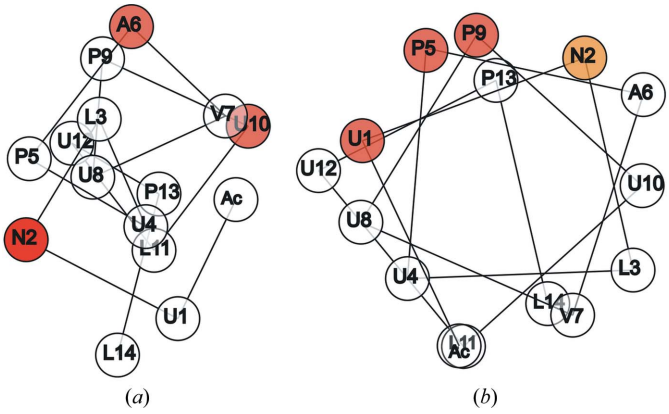

Figure 6
Real helical wheel projections of the crystal structure of mol-*A* (*a*) and of a modelled trichovirin α-helix (*b*). Coloured residues indicate polar groups that are not involved in intramolecular hydrogen bonding: orange for main-chain carbonyl groups in (*a*) and (*b*), red for both carbonyl groups and side chains in (*a*) and yellow only for side chains in (*b*). The N-terminal NH groups and the C-terminal CH_2OH groups, which potentially form intermolecular hydrogen bonds, are not included.

themselves appear to be apolar and free of at least any ordered water.

To investigate the polar/apolar group distribution in trichovirin peptides, we have drawn the real helical wheel for one molecule with the principal helical axis aligned along the viewing direction (Fig. 6*a*). This N- to C-terminal projection shows the curved helical axis and reveals that the carbonyl groups of Asn2, Ala6, Aib10 and the side chain of Asn2 lie on different sides of the helical axis. In the crystal, the side chain and the carbonyl group of Asn2 are intermolecularly hydrogen bonded, while the hydrophilic carbonyl groups of Ala6 and Aib10 do not participate in any hydrogen bonding at all.

Constructing a helical wheel of a modelled α-helical trichovirin (ideal $\varphi/\psi/\omega$ of $-60/-45/180^\circ$; Fig. 6*b*) reveals that the carbonyl groups which do not participate in intramolecular hydrogen bonding (Aib1, Pro5 and Pro9) constitute one side of a functionally amphipathic helix, while the most apolar side chains (Leu3, Val7, Leu11 and Lol14) are opposite and are properly disposed to contact the membrane.

It can be convincingly concluded that the crystal structure determined here shows the structure of trichovirin in a polar environment, not quite inclined to enter the membrane. Nonetheless, the low dipole moment and the strain imposed on the structure by the bending angle facilitate the structural change which enables the antibiotic to function. The authors propose that during the embedding of trichovirin into the membrane, a structural change from a 3_{10}-helix to an α-helix is effected that enables the molecules to become amphipathic and to interact with membranes. Structural flexibility is supported by the slightly different hydrogen-bonding scheme between molecules *A* and *B* and by the fact that the crystal structure of the C-terminal dodecapeptide is a mixed $3_{10}/\alpha$-helix. This proposed structural transition from 3_{10}-helix to α-helix remains to be thoroughly examined.

The authors would like to thank Dr Louic S. Vermeer for his *WHEEL* Perl script, which was used to produce Fig. 6, and Dr Vangelis Daskalakis for computations.

References

Balashova, T. A., Shenkarev, Z. O., Tagaev, A. A., Ovchinnikova, T. V., Raap, J. & Arseniev, A. S. (2000). *FEBS Lett.* **466**, 333–336.
Bansal, M., Kumar, S. & Velavan, R. (2000). *J. Biomol. Struct. Dyn.* **17**, 811–819.
Berman, H. M., Westbrook, J., Feng, Z., Gilliland, G., Bhat, T. N., Weissig, H., Shindyalov, I. N. & Bourne, P. E. (2006). *International Tables for Crystallography*, Vol. *F*, 1st online ed., edited by E. Arnold & M. G. Rossmann, pp. 675–684. Chester: International Union of Crystallography.
Brückner, H. & Koza, A. (2003). *Amino Acids*, **24**, 311–323.
Bruno, I. J., Cole, J. C., Kessler, M., Luo, J., Motherwell, W. D., Purkis, L. H., Smith, B. R., Taylor, R., Cooper, R. I., Harris, S. E. & Orpen, A. G. (2004). *J. Chem. Inf. Comput. Sci.* **44**, 2133–2144.
Chen, V. B., Arendall, W. B., Headd, J. J., Keedy, D. A., Immormino, R. M., Kapral, G. J., Murray, L. W., Richardson, J. S. & Richardson, D. C. (2010). *Acta Cryst.* D**66**, 12–21.
Chen, Y., Mant, C. T., Farmer, S. W., Hancock, R. E., Vasil, M. L. & Hodges, R. S. (2005). *J. Biol. Chem.* **280**, 12316–12329.
Chugh, J. K., Brückner, H. & Wallace, B. A. (2002). *Biochemistry*, **41**, 12934–12941.
Chugh, J. K. & Wallace, B. A. (2001). *Biochem. Soc. Trans.* **29**, 565–570.
DeLano, W. L. (2002). *PyMOL*. http://www.pymol.org.
Di Blasio, B., Pavone, V., Saviano, M., Lombardi, A., Nastri, F., Pedone, C., Benedetti, E., Crisma, M., Anzolin, M. & Toniolo, C. (1992). *J. Am. Chem. Soc.* **114**, 6273–6278.
Diederichs, K. & Karplus, P. A. (1997). *Nature Struct. Biol.* **4**, 269–275.
Engh, R. A. & Huber, R. (2006). *International Tables for Crystallography*, Vol. *F*, 1st online ed., edited by E. Arnold & M. G. Rossmann, pp. 382–392. Chester: International Union of Crystallography.
Evans, P. (2006). *Acta Cryst.* D**62**, 72–82.
Evans, G., Axford, D. & Owen, R. L. (2011). *Acta Cryst.* D**67**, 261–270.
Fox, R. O. & Richards, F. M. (1982). *Nature (London)*, **300**, 325–330.
Gessmann, R., Benos, P., Brückner, H. & Kokkinidis, M. (1999). *J. Pept. Sci.* **5**, 83–95.
Gessmann, R., Brückner, H. & Petratos, K. (2003). *J. Pept. Sci.* **9**, 753–762.
Gessmann, R., Kokkinidis, M. & Brückner, H. (1994). *Z. Kristallogr.* **209**, 597–603.
Guex, N. & Peitsch, M. C. (1997). *Electrophoresis*, **18**, 2714–2723.
Humphrey, W., Dalke, A. & Schulten, K. (1996). *J. Mol. Graph.* **14**, 33–38.
Jia-xing, Y., Woolfson, M. M., Wilson, K. S. & Dodson, E. J. (2005). *Acta Cryst.* D**61**, 1465–1475.
Kabsch, W. (2010). *Acta Cryst.* D**66**, 125–132.
Karle, I. L., Perozzo, M. A., Mishra, V. K. & Balaram, P. (1998). *Proc. Natl Acad. Sci. USA*, **95**, 5501–5504.
Kelley, L. A., Gardner, S. P. & Sutcliffe, M. J. (1997). *Protein Eng.* **10**, 737–741.
Kiess, M. & Brückner, H. (1990). *DECHEMA Biotechnology Conferences*, edited by D. Behrens & P. Kramer, pp. 1155–1158. Weinheim: VCH Verlagsgesellschaft.
Kraft, P., Bergamaschi, A., Broennimann, Ch., Dinapoli, R., Eikenberry, E. F., Henrich, B., Johnson, I., Mozzanica, A., Schlepütz, C. M., Willmott, P. R. & Schmitt, B. (2009). *J. Synchrotron Rad.* **16**, 368–375.
Laskowski, R. A., MacArthur, M. W., Moss, D. S. & Thornton, J. M. (1993). *J. Appl. Cryst.* **26**, 283–291.
Li, A. J. & Nussinov, R. (1998). *Proteins*, **32**, 111–127.

Lucaciu, M., Rebuffat, S., Goulard, C., Duclohier, H., Molle, G. & Bodo, B. (1997). *Biochim. Biophys. Acta*, **1323**, 85–96.
Matthews, B. W. (1968). *J. Mol. Biol.* **33**, 491–497.
McRee, D. E. (1999). *J. Struct. Biol.* **125**, 156–165.
Mouritsen, O. G. & Bloom, M. (1984). *Biophys. J.* **46**, 141–153.
Mukherjee, P. K., Wiest, A., Ruiz, N., Keightley, A., Moran-Diez, M. E., McCluskey, K., Pouchus, Y. F. & Kenerley, C. M. (2011). *J. Biol. Chem.* **286**, 4544–4554.
Paterson, Y., Rumsey, S. M., Benedetti, E., Némethy, G., Scheraga, H. A. (1981). *J. Am. Chem. Soc.* **103**, 2947–2955.
Perrakis, A., Sixma, T. K., Wilson, K. S. & Lamzin, V. S. (1997). *Acta Cryst.* D**53**, 448–455.
Persistence of Vision Pty Ltd (2004). *POV-Ray – The Persistence of Vision Raytracer*. http://www.povray.org/.
Rebuffat, S., Goulard, C. & Bodo, B. (1995). *J. Chem. Soc. Perkin Trans.* **1**, 1849–1855.
Sansom, M. S. (1991). *Prog. Biophys. Mol. Biol.* **55**, 139–235.
Ségalas, I., Prigent, Y., Davoust, D., Bodo, B. & Rebuffat, S. (1999). *Biopolymers*, **50**, 71–85.
Sheldrick, G. M. (2008). *Acta Cryst.* A**64**, 112–122.
Snook, C. F., Woolley, G. A., Oliva, G., Pattabhi, V., Wood, S. F., Blundell, T. L. & Wallace, B. A. (1998). *Structure*, **6**, 783–792.
Solà, J., Helliwell, M. & Clayden, J. (2011). *Biopolymers*, **95**, 62–69.
Taylor, R. (2002). *Acta Cryst.* D**58**, 879–888.
Toniolo, C. & Benedetti, E. (1991). *Trends Biochem. Sci.* **16**, 350–353.
Viterbo, A., Wiest, A., Brotman, Y., Chet, I. & Kenerley, C. (2007). *Mol. Plant Pathol.* **8**, 737–746.
Weiss, M. S. & Hilgenfeld, R. (1997). *J. Appl. Cryst.* **30**, 203–205.
Wiest, A., Grzegorski, D., Xu, B.-W., Goulard, C., Rebuffat, S., Ebbole, D. J., Bodo, B. & Kenerley, C. (2002). *J. Biol. Chem.* **277**, 20862–20868.
Winn, M. D. *et al.* (2011). *Acta Cryst.* D**67**, 235–242.